Supporting Information

Amino acid-based functional additive enables fast polyiodide conversion kinetics for durable Zn-I_2 batteries

Xinran Fu [a, #], Yicai Pan [b, #], Zhixiang Chen [a, #], Fulong Li [a, #], Yongqiang Yang [c], Min Chen [d], Haoran Tu [d], Tianyu Qiu [a], Zhenyue Xing [a], Peng Rao [a], Zhenye Kang [a], Wenjun Zhang [b], Xiaodong Shi [a, *], Lutong Shan [a, e, *], Xinlong Tian [a, *]

[a] School of Chemistry and Chemical Engineering, State Key Laboratory of Tropic Ocean Engineering Materials and Materials Evaluation, Hainan University, Haikou 570228, China

[b] Department of Materials Science and Engineering & Center of Super-Diamond and Advanced Films (COSDAF), City University of Hong Kong, Hong Kong SAR 999077, China

[c] Department of Applied Biology and Chemical Technology, The Hong Kong Polytechnic University, Hong Kong SAR 999077, China

[d] School of Materials Science and Engineering, Dongguan University of Technology, Dongguan 523808, China

[e] Department of Chemical and Biomolecular Engineering, National University of Singapore, 117585, Singapore

* Corresponding authors emails: shixiaodong@hainanu.edu.cn; lutong_shan@nus.edu.sg; tianxl@hainanu.edu.cn

[#] These authors contributed equally.

1. Experimental section

1.1 Commercial reagents

D-Penicillamine (DPL) and Zinc sulfate heptahydrate ($ZnSO_4 \cdot 7H_2O$), were purchased from Aladdin (Shanghai Aladdin Biochemical Technology Co., LTD).

1.2 Preparation of electrolytes

2M $ZnSO_4$ electrolyte was prepared by dissolving 143.78 g $ZnSO_4 \cdot 7H_2O$ in 250 mL deionized water and labeled as ZSO electrolyte throughout the paper. DPL electrolyte was prepared by dissolving 0.1 wt.% (≈8.8 mM) of DPL ($C_5H_{11}NO_2S$) powder into the 2 M $ZnSO_4$ electrolyte. To clarify this calculation process, we provide the detailed steps as follows: For 5 mL of 2 M ZSO electrolyte, its mass was weighed approximately 6.56 g. Thus, 6.56 mg of DPL (0.1 wt.%) was weighed. Given that the molar mass of DPL [M(DPL)] is 149.21 g/mol and the concentration formula is c = n/V (concentration = amount of substance/volume), the concentration of DPL [C(DPL)] was calculated as follows: 0.00656 g ÷ 149.21 g/mol ÷ 0.005 L ≈ 8.8 mM.

1.3 Fabrication of AC@I_2 cathode

Activated carbon@iodine (AC@I_2) materials are prepared by the same iodine fixation method reported in our previous work. Firstly, the I_2 and AC powder are mixed under the mass ratio of 1:1 in a mortar, then the mixed powder is transferred to the glass bottle, calcined in a muffle furnace at 120 ℃ for 6 hours, and the black powder AC@I_2 is obtained after fully cooling. For the preparation of AC@I_2 cathode, the mass of AC@I_2 and Ketjen Black and PTFE powder is fully ground compared to 7:2:1 in the mortar. Then, it is added with deionized water to make a black paste, which is uniformly coated on the surface of stainless-steel mesh (400 mesh) cut into 12 mm diameter, and dried at 40 ℃ for the night. The areal iodine loading for the coin cells used to generate the key electrochemical data in **Figure 3** (e.g., CV, Tafel, EIS, rate capability, and long-term cycling) is approximately 1 mg cm^{-2}. Among them, Under the high current density of 10 A g^{-1}, a iodine loading of around 2.3 mg maintains stable performance over 12,000 long-term cycles.

1.4 Fabrication of Pouch battery

First, the mass of AC@I_2, Ketjen Black and PTFE emulsion as 8:1:1 than in the mortar fully grinding. Secondly, transfer the mixed slurry to the glass plate, roll with a glass stick into a thin sheet of uniform thickness, and air dry naturally in the air. Then, press the dry sheet onto the stainless-steel mesh surface. The mass loading of the iodine cathode can be changed by adjusting the volume of the mixture. Finally, the performance of cathode, separator and Zn anode were assembled into a Pouch battery to test the performance of charging and discharging cycle.

1.5 Material characterizations

The crystal structure and surface functional groups of DPL and ZSO electrolytes were determined by ultraviolet-visible absorption spectra (UV-vis, UV-2700i), Raman spectra (Renishaw inVia) and Fourier transform infrared (FT-IR) spectra (IRTracer-100). X-ray diffraction (XRD, Cu Kα radiation, Rigaku D/max 2500), scanning electron microscopy (SEM, Verios G4 UC, Thermo Fisher Scientific) and atomic force microscope (AFM, Bruker Dimension ICON) were used to characterize and compare the surface morphology of zinc anode before and after immersion in electrolyte. In addition, the reaction mechanism of Zn||AC@I_2 battery during charging and discharging cycle was revealed by in situ UV-vis spectra and in situ Raman spectra.

1.6 Theoretical calculation details

Density Functional Theory (DFT) calculations were performed by using the CP2K package[1]. by using the CP2K package mixed Gaussian and plane-wave scheme[2] and the Quickstep module[3]. The Perdew-Burke-Ernzerhof (PBE) exchange correlation functional[4], Goedecker-Teter-Hutter (GTH) pseudopotential[5], DZVP-MOLOPT-SR-GTH / TZVP-MOLOPT-SR-GTH / TZVP-MOLOPT-GTH basis sets were used to describe the system[3]. A plane-wave energy cut-off and relative cut-off of 400 Ry and 55 Ry have been employed, respectively. The energy convergence criterion was set to 10^{-6} Hartree. The DFT-D3(BJ) level correction for dispersion interactions was applied[6]. Structural optimization was performed using the Limited Memory

Broyden-Fletcher-Goldfarb-Shannon (LBFGS) optimizer, until the maximum force is below 0.00045 Ry/Bohr (0.011 eV/Å). The charge differential density was calculated and plotted through the software Multiwfn[7] and Visual Molecular Dynamics (VMD)[8], respectively. The Gibbs free-energy diagrams were estimated under zero potential (U = 0) by the equation[9]:

$$\Delta G_H = \Delta E_H + \Delta ZPE - T\Delta S$$

during which ΔE_H is the energy change between the reactant and product obtained from DFT calculations, ΔZPE is the change of zero point energy and T and ΔS represents the temperature and change of entropy, respectively. T = 298.15 K was employed in this case.

The molecular dynamics (MD) simulations were conducted in GROMACS software[10]. Water molecules were simulated with SPC/E model. Parameter fitting was performed using the density functional theory (DFT) package Orca[11] under B3LYP exchange-correlation functional with Grimme's DFT-D3(BJ) empirical dispersion correction. The RESP2(0.5) [Non-bonded force field model with advanced restrained electrostatic potential charges (RESP2)] charge combining gas- and liquid-phase (implicit solvent, SMD model) charges were adopted for all molecules in this work calculated using Orca[11] and Multiwfn package[7]. The electrolyte system was initialized using the Packmol package[12]. The MD simulation was firstly performed in the NVT ensemble at temperature (298 K) by using 2 fs time step for 1 ns. Then equilibrium simulation is performed in the NPT ensemble at constant pressure (1 bar) and temperature (298 K) in a cubic box with periodic boundary conditions in all xyz Cartesian directions by using 2 fs time step for 2 ns. Finally, the production simulation is performed in the NVT ensemble at temperature (298 K) by using 2 fs time step for 10 ns. The coordination number of molecules of type i in the first solvation shell surrounding a single molecule of type j is calculated as:

$$N_i = 4\pi n_j \int_0^{R_M} g_{ij}(r) r^2 dr$$

in which RM is the distance of the first minimum following the first peak in the radial distribution function

(RDF), and $gij(r)$is a standard approach for bulk liquid. All the visualizations of MD simulations are implemented by VMD software[8]. The mean square displacement (MSD) of the atom is calculated by the Einstein equation:

$$MSD \equiv \sum_{i}^{n} [(R_i(t) - R_0(t))^2]$$

where R is the atomic coordinates, N is total number of atoms, and t is the time. The diffusion constant (D) is the slope of MSD versus times with a factor of 1/2:

$$D = \frac{MSD}{2t}$$

1.7 Electrochemical characterization

Zn||Zn symmetrical cell is assembled with commercial zinc foil (purity: 99.9%; thickness: 0.1mm) as electrode, glass fiber (Whatman, GF/D) as separator, DPL or ZSO as electrolyte. Zn||Cu half-cell, Zn||Steel mesh cell assembly is similar to a symmetrical cell, the only difference is with copper foil or steel mesh instead of one zinc foil. CA curve, Tafel curve and EIS curve were tested by electrochemical workstation. The activation energy (E_a) of the Zn||Zn cell was calculated via Arrhenius fitting, which is based on the charge transfer resistance (R_{ct}) obtained from electrochemical impedance spectroscopy (EIS) measurements at different temperatures. The cycling performance of Coulomb efficiency and different current densities were tested on the NEWARE battery test system (CT-4008-5V200A-NTFA). The LSV curve is recorded by the Gamry electrochemical workstation.

We use AC@I_2 as the cathode, zinc foil as the anode, glass fiber as the separator, DPL or ZSO as the electrolyte to assemble Zn-I_2 batteries. The Cyclic voltammetry (CV) curves (0.6-1.6 V) and EIS curves (10 mHz-100 kHz) of the Zn||AC@I_2 battery were tested using an electrochemical workstation (CHI660E, Shanghai Chinstruments Co., Ltd). Then the cyclic stability and multiplier performance of the Zn||AC@I_2 battery at 0.6-1.6 V voltage were tested using NEWARE battery test system (CT-4008-5V200A-NTFA). The specific capacity of Zn-I_2 battery was calculated based on the load content of positive active I_2.

Supplementary figures and captions

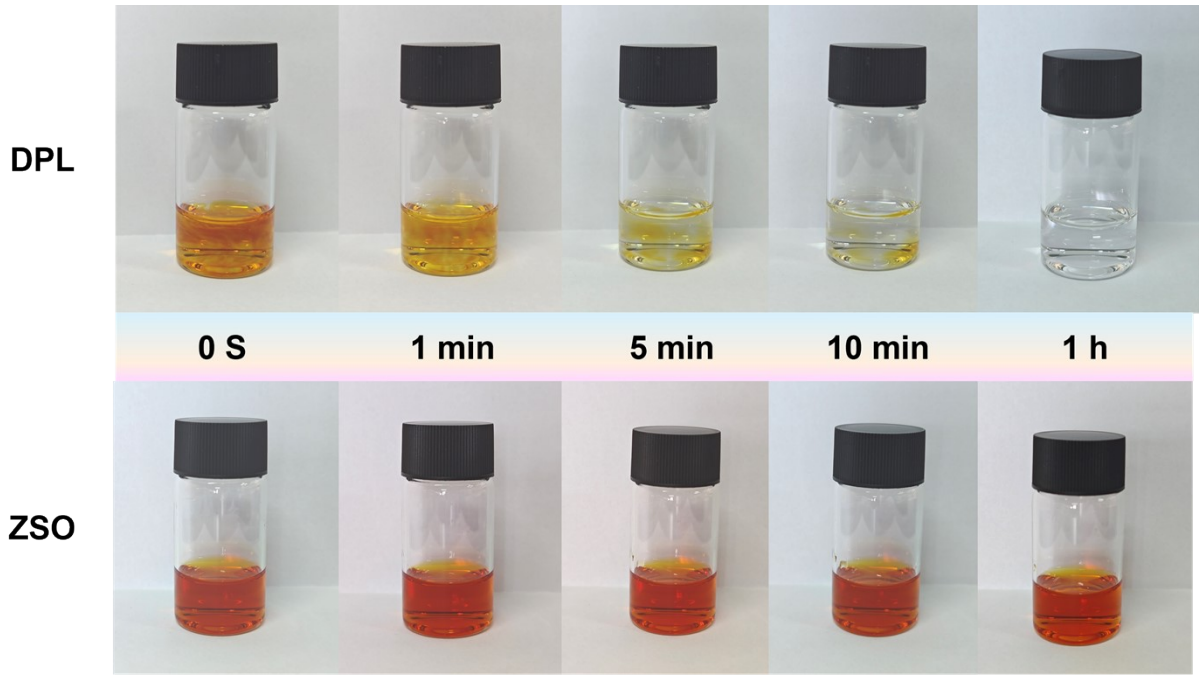

Figure S1 Digital photos of the color change in DPL+I_3^- solution and ZSO+ I_3^- solution for different time.

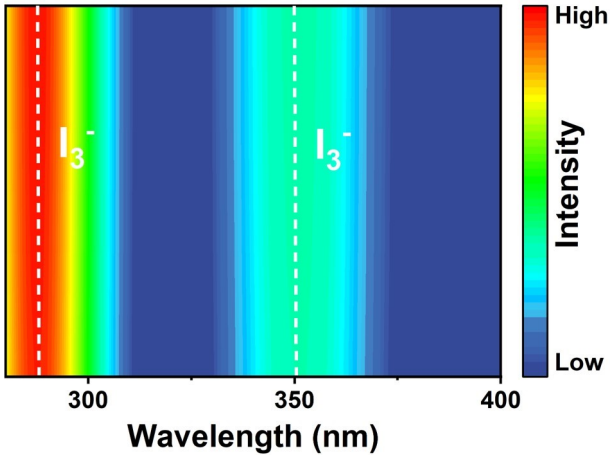

Figure S2 UV-vis absorption spectra of ZSO-containing solution during I_3^- adsorption process.

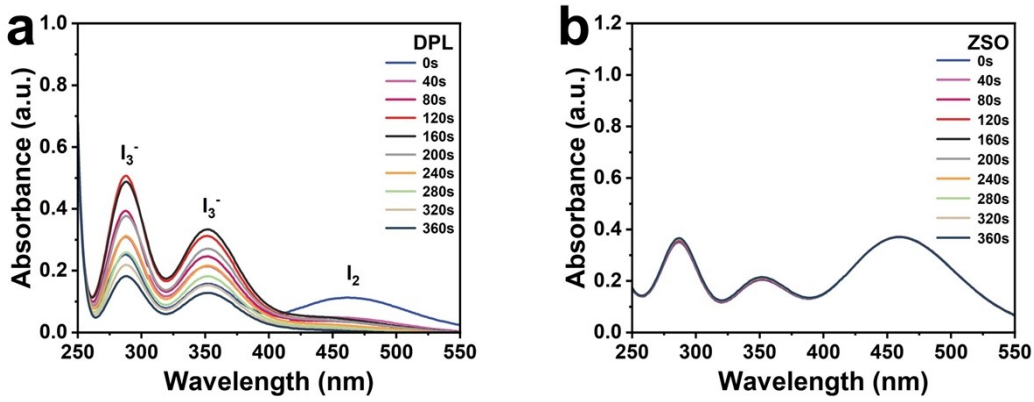

Figure S3 UV-vis absorption spectra of (a) DPL-containing solution and (b) ZSO-containing solution during I_2 adsorption process

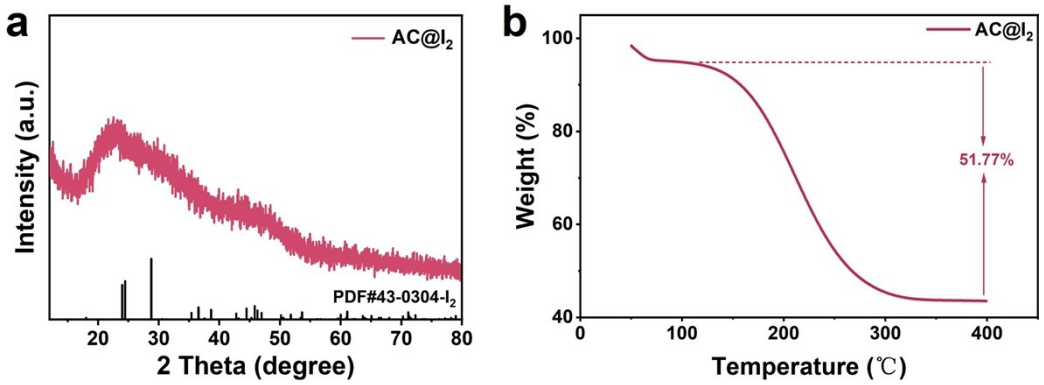

Figure S4 (a) XRD pattern of AC@I_2 composite material; (b) thermogravimetric curve of AC@I_2 composite material.

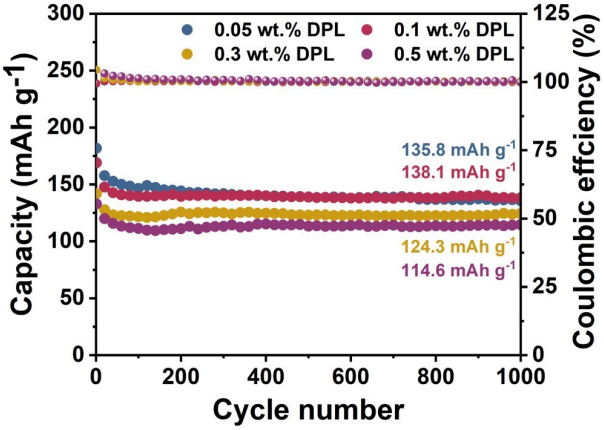

Figure S5 Cycling performance comparison of Zn-I_2 batteries prepared with different content of DPL electrolyte (0.05 wt.%/0.1 wt.%/0.3 wt.%/0.5 wt.%).

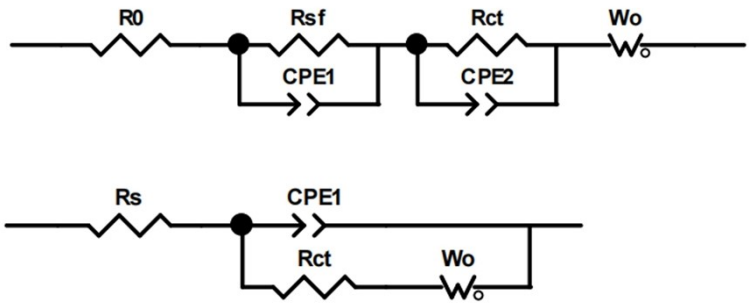

Figure S6 Equivalent circuit diagram of DPL and ZSO electrolyte.

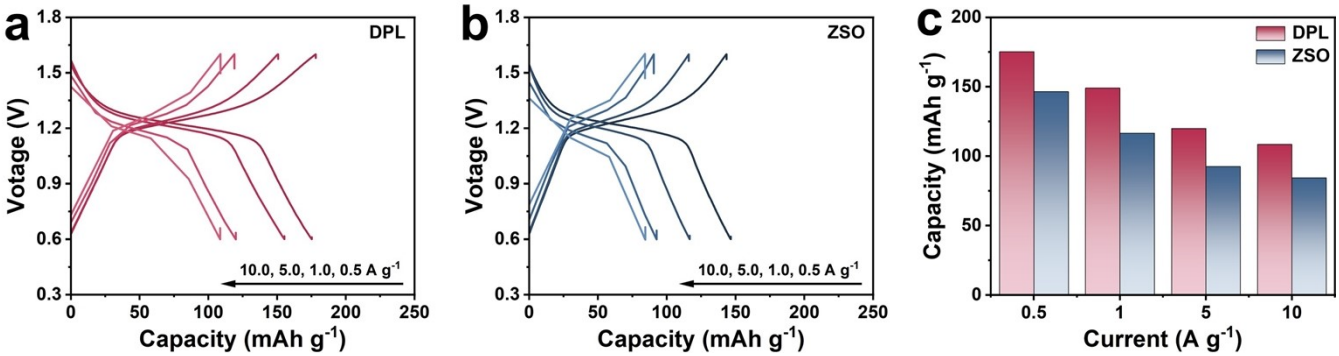

Figure S7 Galvanostatic charge/discharge curves of Zn-I_2 batteries at different current densities in (a) DPL and (b) ZSO electrolytes; (c) The calculated capacity retention rates of Zn-I_2 batteries at different current densities in DPL and ZSO electrolytes.

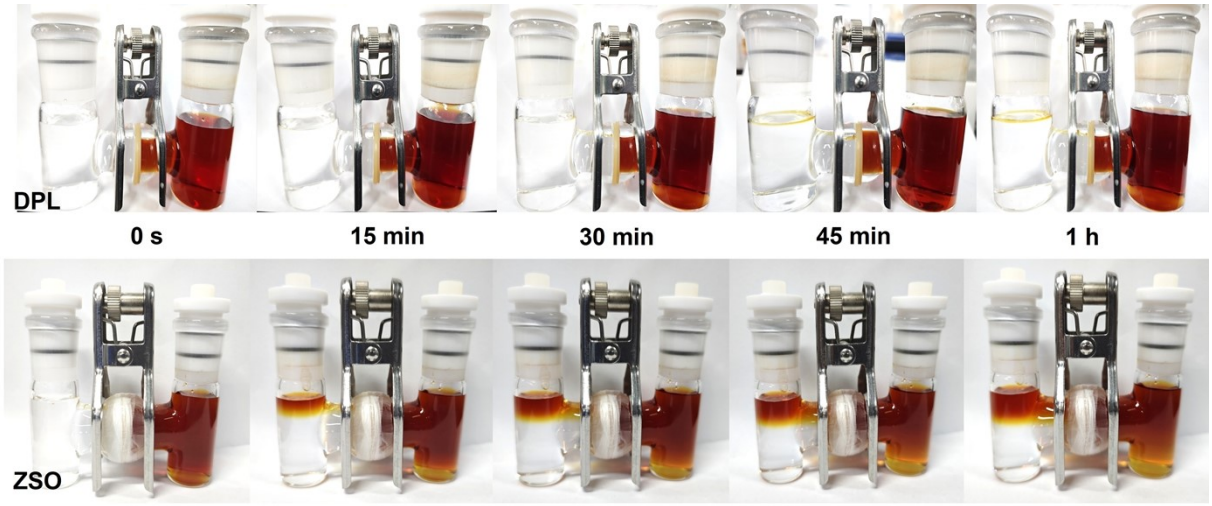

Figure S8 Penetration tests of I_3^- solution through the glass fibre separator to DPL and ZSO electrolytes.

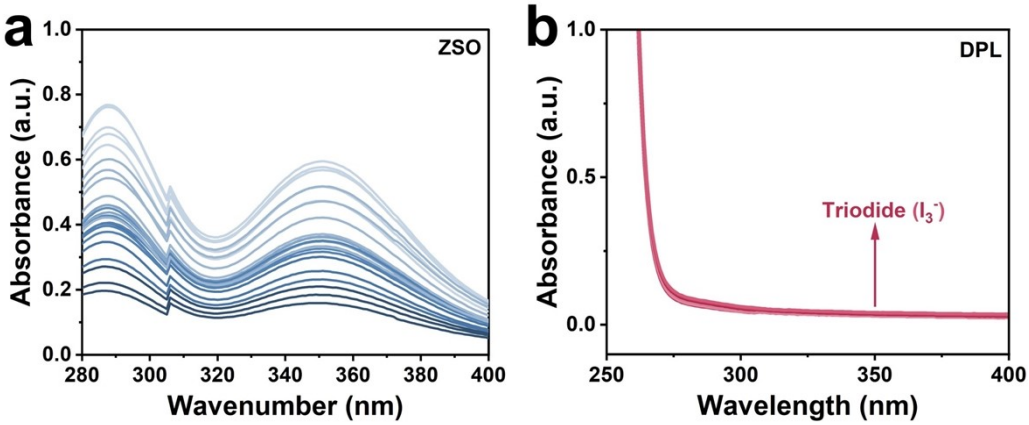

Figure S9 The corresponding UV-vis absorbance intensity of Zn-I_2 batteries during cycling process in (a) ZSO and (b) DPL electrolyte.

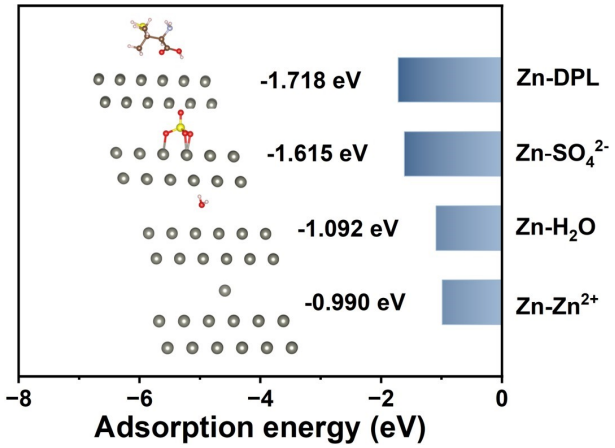

Figure S10 The calculated adsorption energy of DPL, H_2O, SO_4^{2-}, Zn^{2+} on the (002) plane of Zn anode.

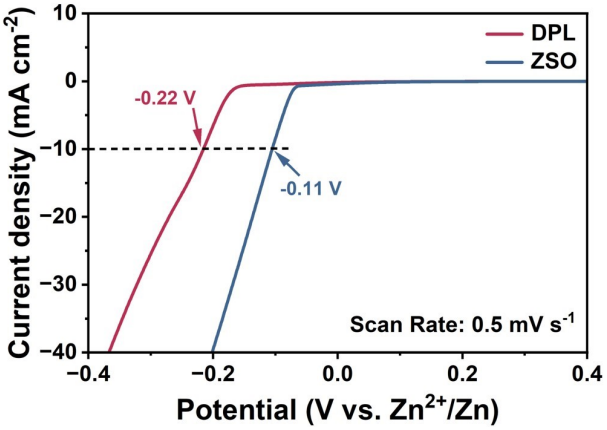

Figure S11 LSV curves of Zn||steel mesh cells in different electrolytes.

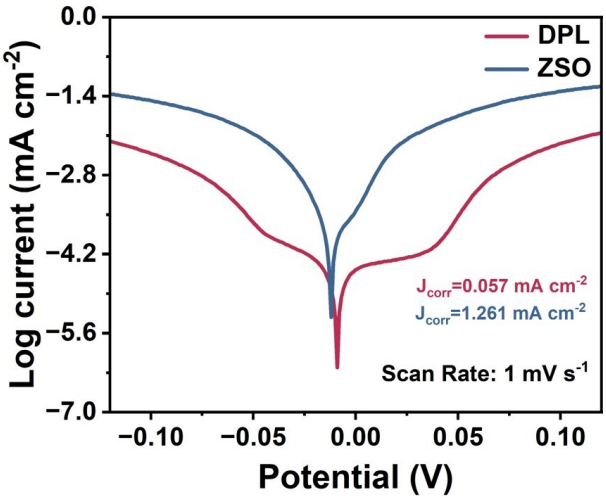

Figure S12 Tafel curves of Zn||Zn cells in DPL and ZSO electrolytes.

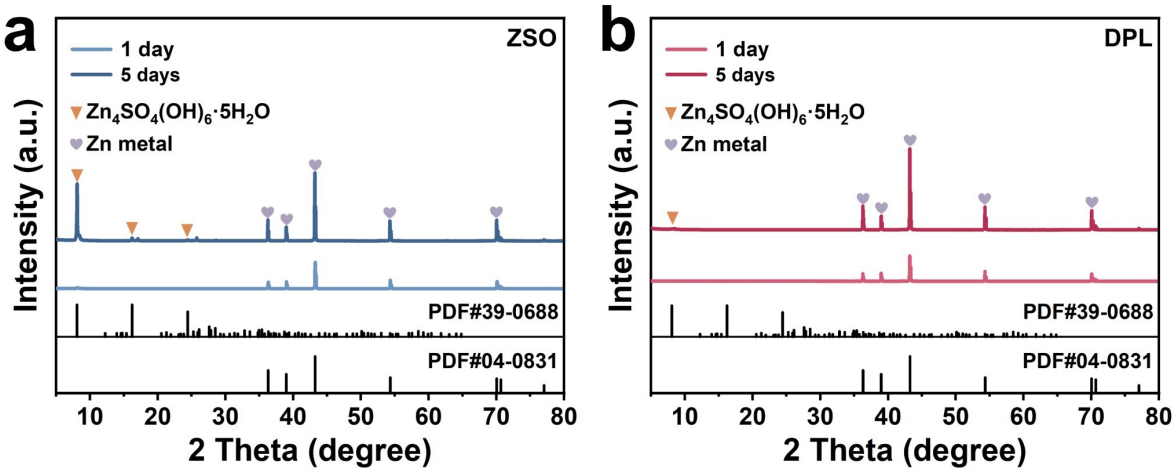

Figure S13 XRD patterns of Zn metal immersed in (a) ZSO and (b) DPL electrolytes for 5 days.

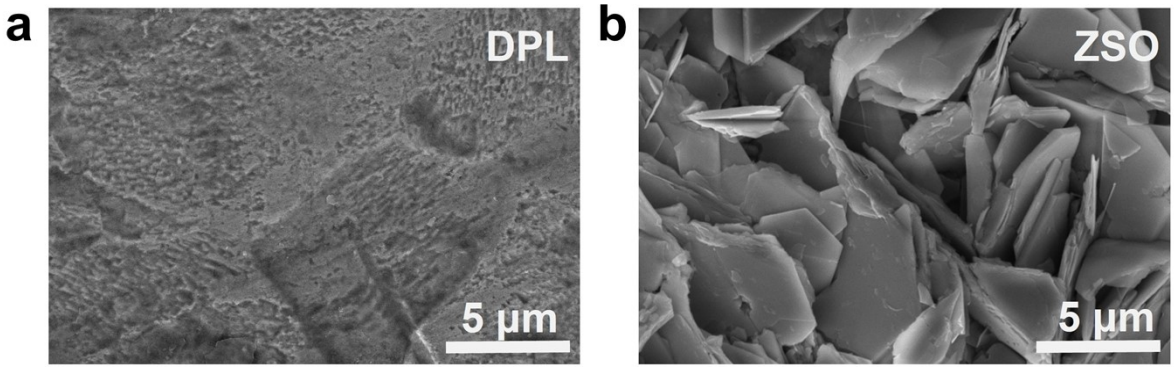

Figure S14 SEM images of Zn anode immersed in (a) DPL and (b) ZSO electrolytes for 5 days

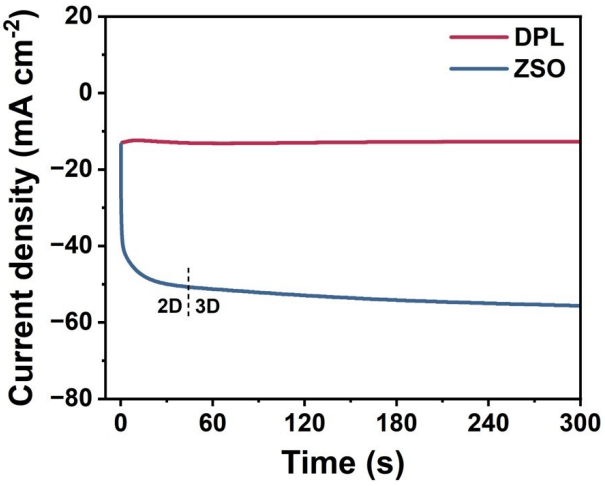

Figure S15 Chronoamperometric (CA) curves of Zn||Zn cells in DPL and ZSO electrolytes

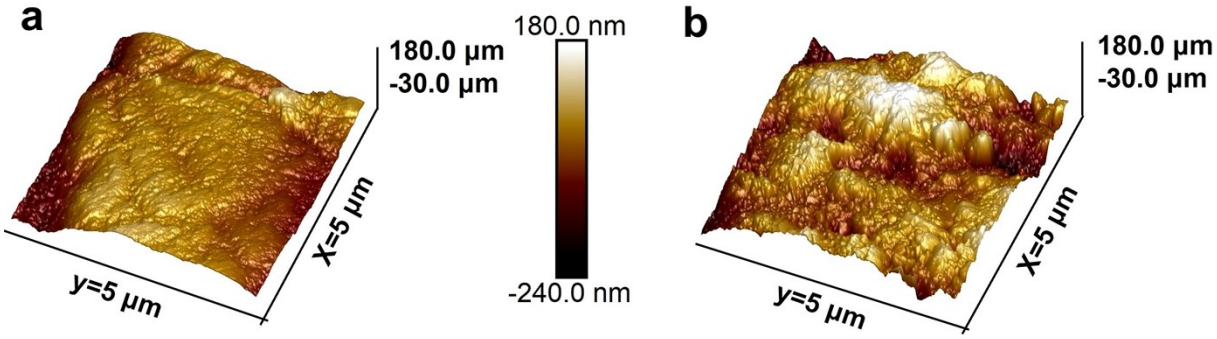

Figure S16 Atomic force microscope (AFM) images of the cycled zinc foils in (a) DPL and (b) ZSO electrolytes.

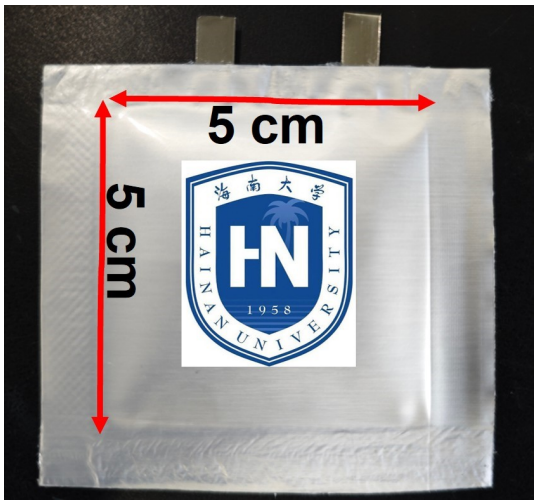

Figure S17 Photo of Zn-I_2 pouch batteries.

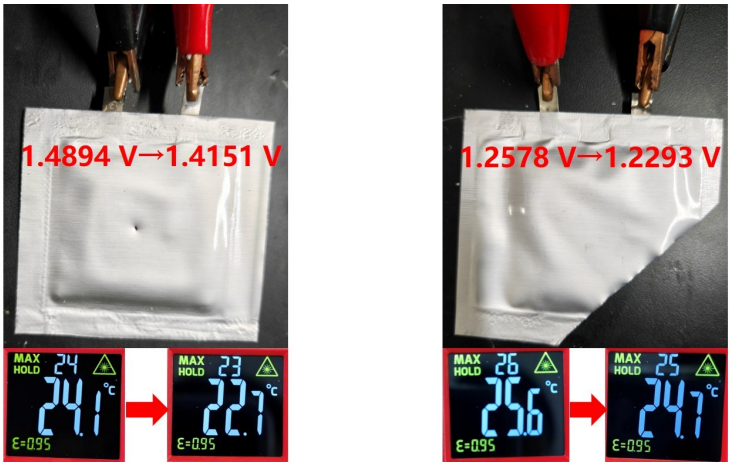

Figure S18 SOC test of pouch cells under puncture and cutting.

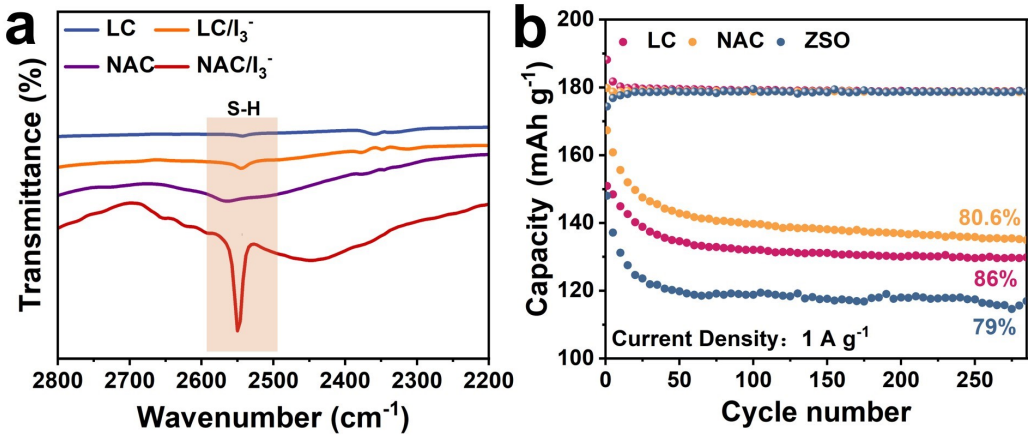

Figure S19 (a) FT-IR spectra of L-cysteine (LC) and N-acetylcysteine (NAC) solution before and after I_3^- adsorption test; (b) Cycling performance comparison of Zn-I_2 batteries prepared with different electrolyte.

Table S1 Comparison of the cycling stability of Zn-I_2 coin cells with different iodine loadings.

Cathodes	Electrolytes	Cycling performances	Ref.
G/PVP@ZnI_2	2 M $ZnSO_4$	80% after 1000 cycles at 1 A g^{-1}	13
AC@I_2	2 M $ZnSO_4$	80% after 20000 cycles at 2 A g^{-1}	14
AC@I_2	0.5 M $ZnSO_4$+0.5 M Li_2SO_4	80.9% after 2700 cycles at 2 A g^{-1}	15
$NiZnN_4/I_2$	2 M $ZnSO_4$	< 70% after 2500 cycles at 0.5 A g^{-1}	16
AC/I_2	ZBF:SN=1:2	75% after 10000 cycles at 10 A g^{-1}	17
cabon@I_2	PZG	~80% after 1000 cycles at 1 A g^{-1}	18
AC@I_2	2 M $ZnSO_4$+0.2 M [EMIM][OAc]	73% after 18000 cycles at 4 A g^{-1}	19
CB-AB@I_2	2 M $ZnSO_4$+20 mM CP5	84.7% after 1000 cycles at 10A g^{-1}	20
odine-containing catholyte	2 M $ZnSO_4$+5 vol% DXm	~80% after 10000 cycles at 5 A g^{-1}	21
AC@I_2	2 M $ZnSO_4$ +0.1 wt.% DPL	81.1% after 3000 cycles at 1 A g^{-1} 87.6% after 12000 cycles at 10 A g^{-1}	This work

Table S2 Comparison of the cycling stability of Zn-I_2 pouch cells with different iodine loadings.

Material	Electrolyte	Current density (A g^{-1})	Cycles	Capacity retention (%)	I_2 loading (mg cm^{-2})	N/P	Ref.
ZnI_2/AC	DCHE	0.05 A g^{-1}	160	82	35	6.35	[22]
S-3@I_3^-	2 M $ZnSO_4$	0.3 A g^{-1}	50	92.4	15	/	[23]
SiBPC/I_2	1 M $ZnSO_4$	0.1 A g^{-1}	100	77.3	16.2	/	[24]
NC-Co/ZnI_2	2 M $ZnSO_4$	/	50	88	/	18.5	[25]
AC-I_2	20 mM $ZnCl_2$+3 M ZnI_2+3 M $ZnAc_2$	1 A g^{-1}	200	70	/	/	[26]
C3/I_2	2 M $ZnSO_4$	0.1 A g^{-1}	60	83	6	/	[27]
ZWCBD@I_2	2 M $ZnSO_4$	0.2 A g^{-1}	150	93	/	/	[28]
I_2@S3-1000	2 M $ZnSO_4$	0.1 A g^{-1}	100	94.3	/	/	[29]
KB	0.1 M I_2+1 M LiI+0.5 M $ZnSO_4$	1 A g^{-1}	200	80	/	/	[30]
AC@I_2	2 M $ZnSO_4$ +0.1 wt.% DPL	0.5 A g^{-1}	100	95.2	14.7	3.8	This work

Table S3 The corresponding charge transfer impedances (R_{ct}) of Zn||Zn symmetric cells in DPL and ZSO electrolytes at different temperatures and the calculated activation energy barriers.

Electrolytes	35 ℃	40 ℃	45 ℃	50 ℃	55 ℃	**Activation energy barriers**
DPL	554	478	388	299	277	**31.2**
ZSO	709	584	498	394	321	**33.2**

References

1. Hutter, J.; Iannuzzi, M.; Schiffmann, F.; VandeVondele, J. cp2k: atomistic simulations of condensed matter systems. *WIRES COMPUT MOL SCI* **2013**, *4* (1), 15-25.

2. Lippert, B. G.; Parrinello, J. H.; Michele. A hybrid Gaussian and plane wave density functional scheme. *Mol. Phys.* **2010**, *92* (3), 477-488.

3. VandeVondele, J.; Krack, M.; Mohamed, F.; Parrinello, M.; Chassaing, T.; Hutter, J. Quickstep: Fast and accurate density functional calculations using a mixed Gaussian and plane waves approach. *Comput. Phys. Commun.* **2005**, *167* (2), 103-128.

4. Goedecker, S.; Teter, M.; Hutter, J. Separable dual-space Gaussian pseudopotentials. *PHYS REV B* **1996**, *54* (3), 1703-1710.

5. Perdew, J. P.; Burke, K.; Ernzerhof, M. Generalized Gradient Approximation Made Simple. *Phys. Rev. Lett.* **1996**, *77* (18), 3865-3868.

6. Grimme, S.; Antony, J.; Ehrlich, S.; Krieg, H. A consistent and accurateab initioparametrization of density functional dispersion correction (DFT-D) for the 94 elements H-Pu. *J. Chem. Phys.* **2010**, *132* (15), 154104.

7. Lu, T.; Chen, F. Multiwfn: A multifunctional wavefunction analyzer. *J. Comput. Chem.* **2011**, *33* (5), 580-592.

8. Humphrey, W.; Dalke, A.; Schulten, K. VMD: Visual molecular dynamics. *J MOL GRAPH* **1996**, *14* (1), 33-38.

9. Bajdich, M.; García-Mota, M.; Vojvodic, A.; Nørskov, J. K.; Bell, A. T. Theoretical Investigation of the Activity of Cobalt Oxides for the Electrochemical Oxidation of Water. *J. Am. Chem. Soc.* **2013**, *135* (36), 13521-13530.

10. Bekker, H.; Berendsen, H.; Dijkstra, E. J.; Achterop, S.; Drunen, R.; van der Spoel, D.; Sijbers, A.; Keegstra, H.; Reitsma, B.; Renardus, M. K. R. Gromacs: A parallel computer for molecular dynamics simulations. *Phys. Comput.* **1993**, *92*, 252-256.

11. Neese, F. The ORCA program system. *WIRES COMPUT MOL SCI* **2011**, *2* (1), 73-78.

12. Martínez, L.; Andrade, R.; Birgin, E. G.; Martínez, J. M. PACKMOL: A package for building initial configurations for molecular dynamics simulations. *J. Comput. Chem.* **2009**, *30* (13), 2157-2164.

13. Zhang, Y.; Wang, L.; Li, Q.; Hu, B.; Kang, J.; Meng, Y.; Zhao, Z.; Lu, H. Iodine Promoted Ultralow Zn Nucleation Overpotential and Zn-Rich Cathode for Low-Cost, Fast-Production and High-Energy Density Anode-Free Zn-Iodine Batteries. *Nano-Micro Lett.* **2022**, *14* (1), 208.

14. Wang, G.; Yao, Q.; Dong, J.; Ge, W.; Wang, N.; Bai, Z.; Yang, J.; Dou, S. In situ Construction of Multifunctional Surface Coatings on Zinc Metal for Advanced Aqueous Zinc-Iodine Batteries. *Adv. Energy Mater.* **2023**, *14* (5), 2303221

15. Wang, K.; Li, H.; Xu, Z.; Liu, Y.; Ge, M.; Wang, H.; Zhang, H.; Lu, Y.; Liu, J.; Zhang, Y.; et al. An Iodine-Chemisorption Binder for High-Loading and Shuttle-Free Zn–Iodine Batteries. *Adv. Energy Mater.* **2024**, *14* (17), 2304110.

16. Qu, W.; Yuan, Y.; Wen, C.; Zhu, J.; Liang, X.; Chen, S.; Li, Z.; Cao, G.; Zhang, M. Ultra-long life and high rate performance zinc-iodine batteries simultaneously enabled by a low-spin electrode. *Energy Storage Mater.* **2025**, *75*, 103993.

17. Xu, H.; Zhang, R.; Luo, D.; Wang, J.; Huang, K.; Chi, J.; Dou, H.; Zhang, X.; Sun, G. Engineering eutectic network for regulating the stability of polyiodides towards high rate and long cycling zinc-iodine batteries. *Energy Storage Mater.* **2023**, *63*, 103019.

18. Zhang, X.; Li, J.; Xie, F.; Xu, X.; Sun, X.; Su, L.; Lu, F.; Zheng, L.; Gao, X. Polyzwitterionic Gel Electrolyte: Dual Optimization of Polyiodide Shuttle Suppression and Anode Stabilization in Aqueous Zn-I_2 Batteries. *Adv. Funct. Mater.* **2025**, 2505132.

19. Xiao, T.; Yang, J. L.; Zhang, B.; Wu, J.; Li, J.; Mai, W.; Fan, H. J. All-Round Ionic Liquids for Shuttle-Free Zinc-Iodine Battery. *Angew. Chem. Int. Ed.* **2024**, *63* (8), e202318470.

20. Wu, X.; Wang, W.; Chen, X.; Xie, J.; Li, X.; Li, L.; Zhao, M.; Li, C.; Piao, Y.; Chen, M. Reconfiguring Zn^{2+} Solvation Structures and Modulating the Inner Helmholtz Plane Via Janus Supramolecules. *Adv. Funct. Mater.* **2024**, *35* (15), 2419795.

21. Zha, C.; Chen, X.; Guo, W.; Lv, Y.; Wu, Y.; Pan, J.; Hang, Y.; Li, J.; Wang, S.; Wang, L. Introducing p-Band Center to Promote p/p-π* Orbital Hybridization for High-Performance Aqueous Zinc-Iodine Batteries Toward Flexible Wearable Devices and Seawater Electrolyte Applications. *Adv. Funct. Mater.* **2025**, e16000.

22. Huang, X.; Pan, T.; Zhang, B.; Wang, J.; Hu, T.; Duan, A.; Luo, S.; Zhao, B.; Li, M.; Lin, Y.; et al. Functionally Segregated Ion Regulation Enables Dual Confinement Effect for Highly Stable Zinc-Iodine Batteries. *Adv. Mater.* **2025**, *37* (30), 2500500.

23. Zhang, L.; Luo, K.; Gong, J.; Zhou, Y.; Guo, H.; Yu, Y.; He, G.; Gohy, J. F.; Parkin, I. P.; Hofkens, J.; et al. Unlocking Durable and Sustainable Zinc-Iodine Batteries via Molecularly Engineered Polyiodide Reservoirs. *Angew. Chem. Int. Ed.* **2025**, *64* (30), e202506822.

24. Jia, X.; Tian, J.; Zhang, Q.; Wan, J.; Song, H.; Xie, Y.; Liu, J. Engineering Electron Cloud Density to Achieve Bifunctional Electrophilic Hosts for Aqueous Zn-I_2 Batteries with Ultrahigh Rate Property and Cycling Stability. *Adv. Funct. Mater.* **2025**, e12022.

25. Ma, J.; Azizi, A.; Zhang, E.; Zhang, H.; Pan, A.; Lu, K. Unleashing the high energy potential of zinc-iodide batteries: high-loaded thick electrodes designed with zinc iodide as the cathode. *Chem. Sci.* **2024**, *15* (12), 4581-4589.

26. Yin, D.; Li, B.; Zhao, L.; Gao, N.; Zhang, Y.; Feng, J.; Cui, X.; Xiao, C.; Su, Y.; Xi, K.; et al. Polymeric Iodine Transport Layer Enabled High Areal Capacity Dual Plating Zinc-Iodine Battery. *Angew. Chem. Int. Ed.* **2024**, *64* (6), e202418069.

27. Guo, X.; Xu, H.; Qiu, Z.; Li, Q.; Li, N.; Yang, Z.; Li, W.; Lian, Y.; Li, Q.; Sui, Y.; et al. Heteroatom-Modulated Asymmetric Cobalt Single-Atom Catalysts on MOF-Derived Carbon Enabling Durable Zinc-Iodine Batteries. *Adv. Mater.* **2025**, e14035.

28. Zhao, R.; Ding, T.; Zhang, H.; Lu, K.; Lu, S. Zwitterionic carbon/binder domain enabling efficient zinc ion percolating network in shuttle-free Zn I_2 batteries. *Chem. Eng. J.* **2025**, *517*, 164508.

29. Li, Y.; Guo, X.; Wang, S.; Sun, W.; Yu, D.; Li, N.; Zhou, H.; Zhang, X.; Pang, H. Nano/Micro Metal-Organic Framework-Derived Porous Carbon with Rich Nitrogen Sites as Efficient Iodine Hosts for Aqueous Zinc-Iodine Batteries. *Adv. Sci.* **2025**, *12* (26), 2502563.

30. Su, T.; Ren, W.; Xu, M.; Xu, P.; Le, J.; Ji, X.; Dou, H.; Sun, R.; Chen, Z. In Situ Construction of Bionic Self-Recognition Layer for High-Performance Zinc-Iodine Batteries. *Adv. Energy Mater.* **2024**, 2401737.